Using Derivatives to Compare Cortical Waves Across Preparations

KAY A. ROBBINS
Department of Computer Science and Cajal Neuroscience Research Center,
The University of Texas at San Antonio, 6900 N. Loop 1604 West, San Antonio, Texas 78249
krobbins@cs.utsa.edu

DAVID M. SENSEMAN
Department of Biology and Cajal Neuroscience Research Center,
The University of Texas at San Antonio, 6900 N. Loop 1604 West, San Antonio, Texas 78249
senseman@utsa.edu

Abstract. Visual stimulation evokes waves of depolarization that propagate within and between cytoarchitectually distinct cortical areas in the turtle visual cortex. These waves appear to reflect underlying low-dimensional characteristics that can be captured using Karhunen-Loéve (KL) decomposition. This paper compares structure across *in vivo*, *in vitro* and simulated preparations of turtle visual cortex using derivative-response relationships. The derivatives of the projections on the low-order KL modes exhibit distinguishing characteristics based on the stimulus. The derived modes corresponding to these derivatives provide a low-order approximation to the initial response with structure similar to that of a traveling wave.

Keywords: cortical wave, KL decomposition, traveling wave

1. Introduction

In turtles, visual stimulation evokes a complex wave of depolarization within the cerebral cortex that originates in the rostral pole of the dorsal cortical area where the cortex receives direct afferent projections from the lateral geniculate complex of the thalamus. Waves evoked by visual stimulation propagate at a relatively uniform velocity from the rostral pole into the caudal pole of dorsal cortex. Waves with the same qualitative features have been observed for *in vitro* preparations [7], *in vivo* preparations [5] and for model simulations [35] of the turtle visual cortex. The current study compares structural features of the waves across preparations in these three different realizations.

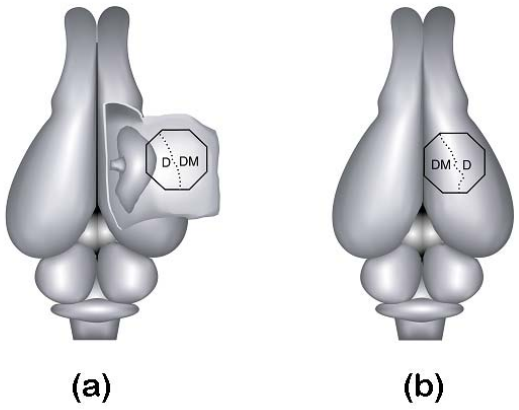

Figure 1: Schematic of the recording area for the *in vitro* (a) and *in vivo* (b) preparations.

Fig.1a shows a schematic of the *in vitro* experiments [6] in which the brain and the attached eyes were surgically removed. To facilitate optical recording, the cortical sheet was freed at the midline and folded flat against the transparent bottom of the recording chamber, taking care not to disturb the normal input from the eye. To monitor cortical activity, the cortical sheet was stained with an absortion voltage-sensitive dye (VSD) and trans-illuminated for optical

recording. Fig. 1b shows a schematic of the *in vivo* experiments [7] in which the surface of the brain was exposed by a craniotomy and partially deafferented by sectioning the spinal cord. The cortical tissue was stained with a fluorescent voltage-sensitive dye and excited using an epi-illumination system. Both experiments recorded with a 464-element silicon photodiode array that served as a fast video camera ($\leq$ 1 ms/frame) with moderate spatial resolution.

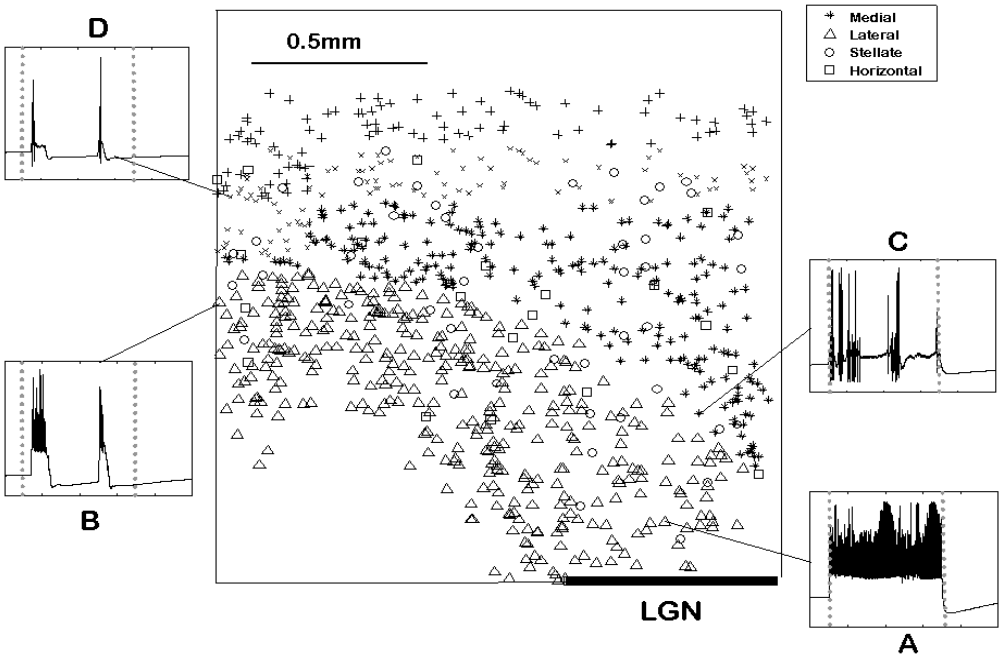

Figure 2: Schematic of neurons in the NGU numerical model.

Fig. 2 shows a schematic of the physiologically-based numerical model of the turtle visual cortex developed by Nenadic et al. [4]. The NGU simulation uses compartmental models of four neuronal types: lateral pyramidal cells (triangles), medial pyramidal cells (stars), stellate cells (circles) and horizontal cells (squares). The distribution, characteristics and connectivities of the cells were based on experimental measurements. The cortex model was driven by a linear array of integrate-and-fire lateral geniculate cells (LGN). In addition to the neuronal distributions, Fig. 2 shows 5-sec time traces of 4 neurons from a trial in which a constant

stimulus was applied to all of the LGN neurons for 3 seconds. Dotted vertical gray lines on each trace mark the starting and stopping points of the stimulus. Notice that the pyramidal neurons closest to the LGN (e.g., A and C) exhibit more vigorous firing patterns than neurons of the same type located more caudally (e.g., B and D). Furthermore, the lateral cells (e.g., A and B) exhibit more vigorous firing patterns than their medial counterparts (e.g., C and D). The initiation of activity at lateral neuron A occurs immediately after stimulus onset, while the activity at lateral neuron B shows a delay that is consistent with an initial wave of activation sweeping the cortex. These general features appear in the response to other types of stimuli as well. Notice that neurons B, C and D show secondary peaks of response roughly 2 seconds after the initial stimulus, while A is continuously activated. These secondary peaks correspond to reexcitation or secondary waves of excitation that sweep through the cortex.

Experiment	**Sampling Rate**	**Trials**	**Stimuli**	**Samples/Trial**
In vitro	353 hz	9	diffuse flashes (100 ms)	576
		17	spots on retinal midline (100 ms)	576
In vivo	1000 hz	5	looming ball	5000
		4	LED 3 sec flash	5000
		2	LED train at 5.8 hz	5000
		2	LED train at 11 hz	5000
Model	1000 hz	10	LGN patches (20 adjacent neurons)	1500
		1	diffuse flashes	1500
		1	LED 3 sec flash	5000
		1	LED train at 5.8 hz	5000
		1	LED train at 11 hz	5000

Table 1: A summary of the trials used for the different preparations.

Although the three experimental setups and stimulus presentations are very different, the basic features of the initial response wave are similar in the three configurations. Table 1 summarizes the trials that are used in the analysis for this paper. The next section reviews KL

decomposition and introduces "derived modes." The final section compares the results for the three experimental preparations.

2. Derivative relationships in KL decomposition

Our analysis of the wave motion first reduces the size of the response space by performing KL decomposition and then examines derivative relationships in the reduced space. For signals that are sampled at discrete points in space and time, the measured response $\mathbf{U} = (u_{x,t})$ can be collected in an $L \times N$ matrix where $x = 1..L$ and $t = 1..N$ represent the sample numbers in space and time, respectively. The discrete proper orthogonal decomposition of $\mathbf{U}$ is:

$$\mathbf{U} = \sum_{k=1}^{r} \alpha_k \varphi^k (\psi^k)^T \qquad (1)$$

where r is the rank of $\mathbf{U}$, the φ^k's are $L \times 1$ orthonormal vectors representing spatial basis functions, and the ψ^k's are $N \times 1$ orthonormal vectors representing temporal basis functions. The φ^k's satisfy $\mathbf{R}\varphi^k = \lambda_k \varphi^k$ where $\mathbf{R} = \mathbf{U}\mathbf{U}^T$ and $\lambda_k = \alpha_k{}^2$. The φ^k's are also the modes or spatial basis functions computed by KL decomposition [2].

The temporal basis function ψ^j can be obtained by left multiplying Eq. (1) by the transpose of φ^j:

$$(\varphi^j)^T \mathbf{U} = \sum_{k=1}^{r} \alpha_k (\varphi^j)^T \varphi^k (\psi^k)^T = \sum_{k=1}^{r} \alpha_k \delta_{j,k} (\psi^k)^T = \alpha_j (\psi^j)^T$$

Taking the transpose of this equation and dividing by α_j gives:

$$\psi^j = \alpha_j{}^{-1} \mathbf{U}^T \varphi^j \qquad (2)$$

Similary the φ^j's can be recovered by multiplying Eq. (1) by ψ^j:

$$\mathbf{U}\psi^j = \sum_{k=1}^{r} \alpha_k \varphi^k (\psi^k)^T \psi^j = \sum_{k=1}^{r} \alpha_k \varphi^k \delta_{k,j} = \alpha_j (\varphi^j)$$

or:

$$\varphi^j = \alpha_j{}^{-1} \mathbf{U} \psi^j \qquad (3)$$

Eq. (2) and Eq. (3) show that φ^j and ψ^j are duals of each other in the sense that one can be obtained from the other by projection on the original data set. If there are fewer time snapshots (N) than spatial points (L), it is more efficient to find the ψ^j's first [2].

We exploit the duality relationship in a slightly different context. We have observed that the time derivatives $d\psi^p/dt$ are correlated with ψ^q for certain *p* and *q*. We obtain *derived spatial basis functions* by assuming that the $d\psi^p/dt$ are temporal modes and use relationship (3) to compute corresponding spatial modes. We then examine how these *derived spatial modes* are related to the spatial modes obtained from the original KL decomposition. The spatial basis function derived by projecting the time derivative of ψ^j on the data set are $(\varphi^j)' = \alpha_j{}^{-1} \mathbf{U}\, d\psi^j/dt$. This paper focuses on the behavior of $d\psi^1/dt$ and its relationship with modes ψ^q for $q > 1$.

3. Results

As described in [8], we concatentate the responses for a collection of stimuli in a preparation and perform a KL decomposition on the composite, to obtain a "global basis". The "global" decomposition is not equivalent to averaging trials before performing KL decomposition. Rather, it is a way to create a common basis so that different trials from the same preparation can be directly compared. An overbar indicates basis functions computed from a

dataset of concatenated trials for the preparation. A prime indicates differentiation with respect to time.

While the details differ quantitatively, the global KL decomposition in all three realizations gives a low-dimensional modal representation dominated by a large single-signed spatial basis function, $\overline{\varphi}^1 = \overline{M}^{1,1}$. We use the notation $\overline{M}^{i,j}$ to denote a spatial basis function with i extrema aligned with the major axes of $\overline{M}^{1,1}$ and j relative extrema aligned with the minor axes of $\overline{M}^{1,1}$ [8]. The modal notation is used because, while $\overline{M}^{1,1}$ always corresponds to the largest KL mode, $\overline{\varphi}^1$, the $\overline{M}^{1,2}$ mode corresponds to $\overline{\varphi}^2$ for the model, to mode $\overline{\varphi}^3$ for the *in vitro* data, and to mode $\overline{\varphi}^4$ for the *in vivo* data. We use $\overline{P}^{i,j}$ to denote the projection of the data set on $\overline{M}^{i,j}$, and $(\overline{P}^{i,j})'$ to denote the time derivative of $\overline{P}^{i,j}$. We represent the mode derived from $(\overline{P}^{i,j})'$ by $(\overline{M}^{i,j})'$.

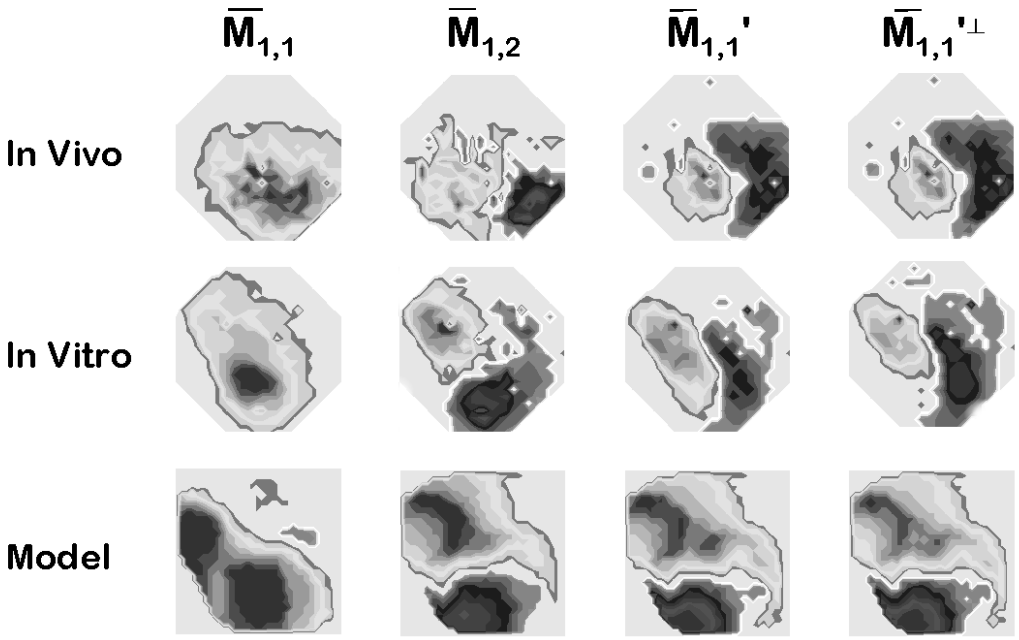

Figure 3: A comparison of the structure of the KL modes and first-order derived modes.

The leftmost column of Fig. 3 shows $\overline{M}^{1,1}$ for the three experimental preparations. The model appears to have a bimodal $\overline{M}^{1,1}$ due to the gray scale color scheme, but in fact, the two dark areas are of the same sign. The second column shows $\overline{M}^{1,2}$ for the different preparations. In each case, $\overline{M}^{1,2}$ has positive and negative extrema separated by a zero response region. The extrema are aligned roughly along the principal axis of $\overline{M}^{1,1}$. We also observed in our data analysis that $\overline{P}^{1,2}$ for individual trials appears to be highly correlated with $(\overline{P}^{1,1})'$, the time derivative of the projection of the data set on $M^{1,1}$. Additionally, $(\overline{P}^{1,1})'$ appears to clearly distinguish response characteristics. For example, trials in both the *in vivo* and model preparations that consisted of LED trains at a specified frequency had a $(\overline{P}^{1,1})'$ with power spectrum dominated by that frequency.

The middle two columns of Fig. 3 compare $\overline{M}^{1,2}$ with $(\overline{M}^{1,1})'$, the basis function derived from $(\overline{P}^{1,1})'$. The rightmost column of Fig. 3 shows the component of $(\overline{M}^{1,1})'$ that is orthogonal to $\overline{M}^{1,1}$. A comparison of columns 3 and 4 of Fig. 3 show that $(\overline{M}^{1,1})'$ is closely aligned with $(\overline{M}^{1,1})'^{\perp}$ indicating that $(\overline{M}^{1,1})'$ is nearly orthogonal to $\overline{M}^{1,1}$. The pair $\overline{M}^{1,1}$ and $(\overline{M}^{1,1})'^{\perp}$ span a two-dimensional space that appears to capture the main features of the initial wave motion.

A translationally invariant system (e.g., traveling waves in a homogeneous unbounded or periodic domain) has sinusoidal KL modes [2]. Sinusoidal basis functions satisfy simple derivative relationships at all orders, capturing the fact that basis functions come in pairs and are phase offsets of each other. The turtle cortex is not translationally-invariant, nor do its basis images represent sinusoidal functions. Yet, the derivative relationships suggest that the global structure of the response wave can be analyzed in terms of a few low order KL modes that are dominated by a traveling wave structure. Ermentrout [1] has analyzed several one-dimensional

neural network models with traveling wave solutions and related the velocity of the wave to the strength of the synaptic coupling. The derived modes provide a mechanism for similar studies of traveling waves in experimental data and nonhomogeneous cortical models.

Acknowledgements: We thank L. Cohen, D. Kleinfeld and P. Mitra for permission to use their *in vivo* data sets. We are also grateful to P. Ulinski, B. Ghosh and Z. Nenadic for allowing us to use their model of the turtle cortex. This work was supported by the NIH (G12 RR13646), the NSF (ACI-9721348), the ONR (N00014-97-0029) and the UTSA Office of the Provost.

References:

[1] B. Ermentrout, The analysis of synaptically generated traveling waves, J. Comp. Neuroscience 5 (1998) 191-208.

[2] M. Kirby, Geometric Data Analysis (John Wiley & Sons, 2001).

[3] Z. Nenadic, B. Ghosh and P. Ulinski, Modeling and estimation problems in the turtle visual cortex, IEEE Trans Biomed. Eng. 49 (2002) 753-762.

[4] Z. Nenadic, B. Ghosh and P. Ulinski, Propagating waves in visual cortex: A large-scale model of turtle visual cortex, J. of Computational Neuroscience (in press).

[5] J. Prechtl, L. Cohen, B. Pesaran, P. Mitra and D. Kleinfeld, Visual stimuli induce waves of electrical activity in turtle cortex, PNAS 94 (1997) 7621-7626.

[6] D. Senseman, Spatiotemporal structure of depolarization spread in cortical pyramidal cell populations evoked by diffuse retinal light flashes, Visual Neuroscience 16 (1999) 65-79.

[7] D. Senseman and K. Robbins, Modal behavior of cortical neural networks during visual processing, J Neuroscience 19 (1999) RC3, 1-7.

[8] D. Senseman and K. Robbins, High-speed VSD imaging of visually evoked cortical waves: Decomposition into intra- and intercortical wave motion, J. Neurophysiology 87(3) (2002) 1499-1514.

Kay Robbins is a Professor at the University of Texas at San Antonio in the Department of Computer Science. Her research focuses on visualization and analysis of multimedia data sets. She collaborates with experimental scientists in the life and physical sciences to use visualization tools on real data. She holds a BS and PhD in Mathematics from the Massachusetts Institute of Technology.

David Senseman received his BS degree in Zoology from Kent State University and his Masters and Doctoral degrees in Biology from Princeton University. During his Post-doctoral fellowship in Biophysics at the University of Pennsylvania, he worked in Brian Salzberg's lab where he learned the "art" of voltage-sensitive dye (VSD) imaging. Since moving to the University of Texas at San Antonio in 1983, he has used VSD imaging to study sensory processing in cortical structures from a variety of mammalian and non-mammalian vertebrates.